Supplementary Information for manuscript

Processing of biomass burning aerosol in the Eastern Mediterranean during summertime

A. Bougiatioti[1], I. Stavroulas[2], E. Kostenidou[3], P.Zarmpas[2], C. Theodosi[2], G. Kouvarakis[2], F. Canonaco[4], A.S.H. Prévôt[4], A. Nenes[1,3,5], S.N. Pandis[3,6] and N. Mihalopoulos[2,3]

[1]School of Earth and Atmospheric Sciences, Georgia Institute of Technology, Atlanta, GA, USA

[2] Environmental Chemical Processes Laboratory, University of Crete, 71003 Crete, Greece

[3] Institute of Chemical Engineering Sciences (ICE-HT), FORTH, Patras, Greece

[4] Laboratory of Atmospheric Chemistry, Paul Scherrer Institute, 5232 Villigen PSI, Switzerland

[5] School of Chemical and Biomolecular Engineering, Georgia Institute of Technology, Atlanta, GA, USA

[6] Department of Chemical Engineering, Carnegie Mellon University, Pittsburgh, USA

SI-1 Backtrajectory analysis and MODIS images

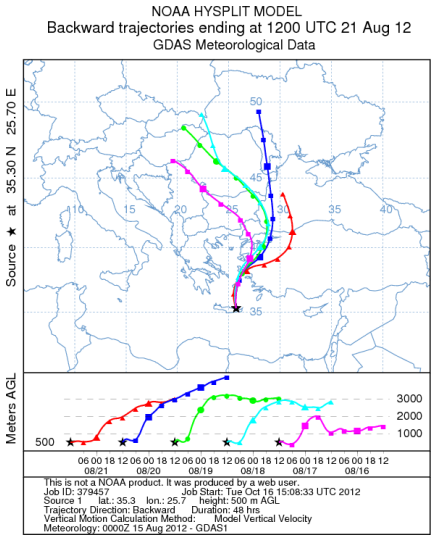

(a1)

(a2)

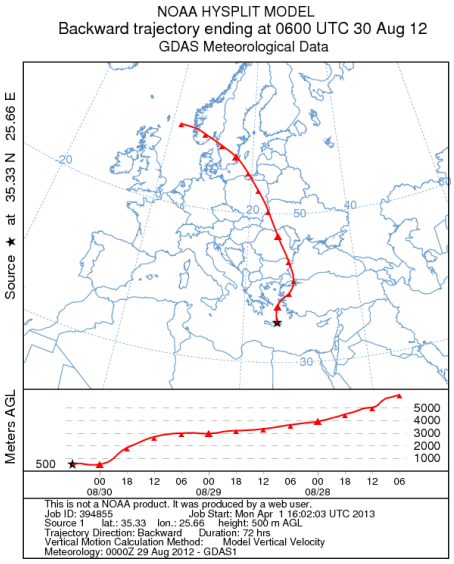

(b1)

(b2)

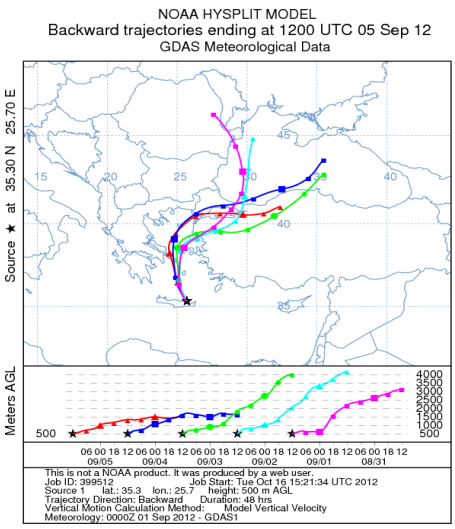

(c1)

(c2)

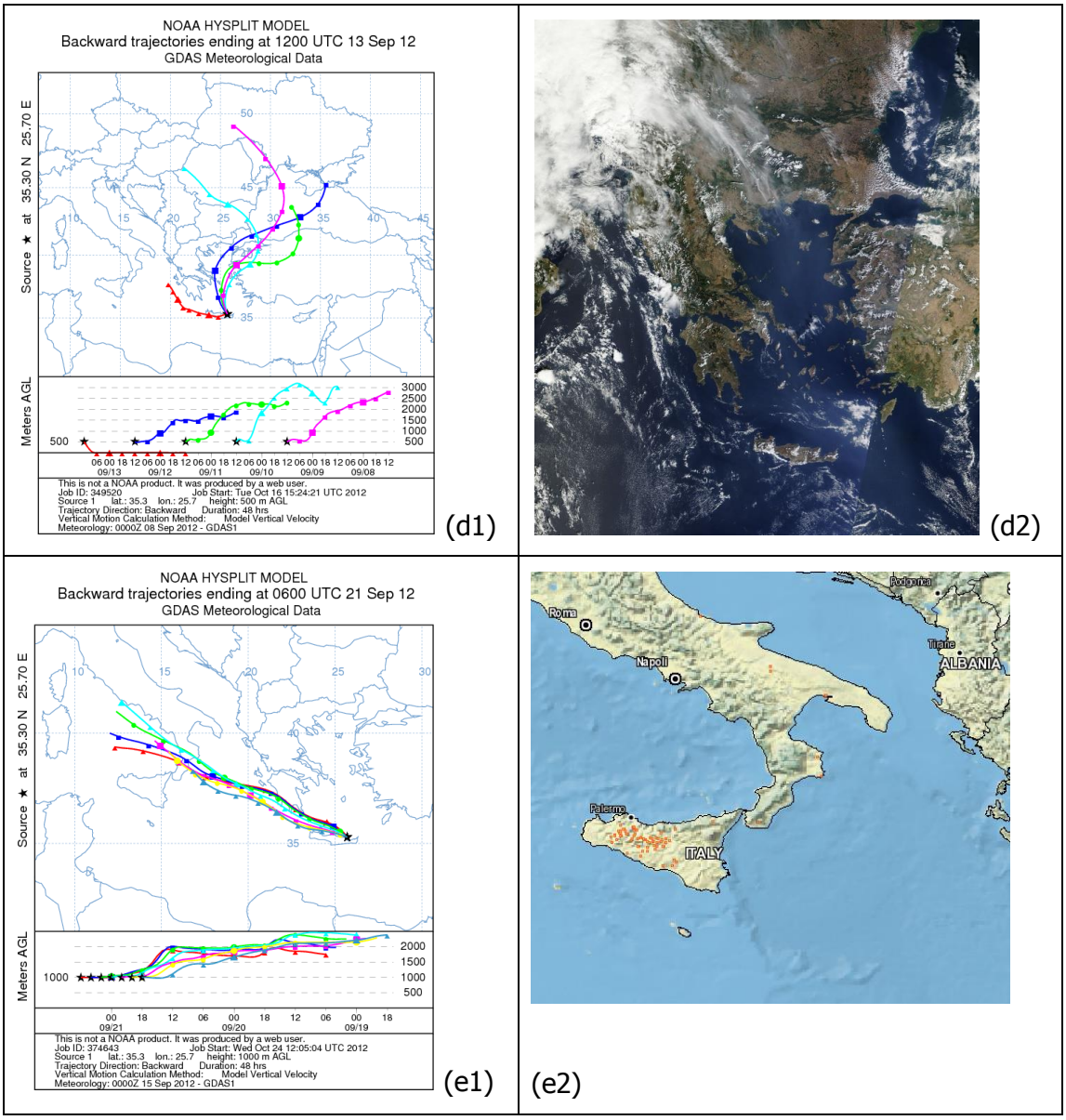

Figure SI-1.1: Wildfires locations derived from backtrajectory analysis (HYSPLIT) and verification by MODIS images and FIRMS Web Fire Mapper: (a) Chios, (b) Dalmatian Coast, (c) Euboea, (d) Andros, and (e) Sicily.

SI-1.2 ACSM tracers during the fire events

The chemical nature of the aerosol was also investigated by examining the dependence of f_{44} versus f_{60}, as well as organic fragments at m/z 43 and 44, shown for the whole measurement period (Figure SI-1.2). According to Cubison et al.[1] f_{60} has consistent background level values around 0.3% in OA with negligible BB

influence, while BB plume measurements exhibit apparent scatter with higher of f_{60} values, with plumes exhibiting a trend toward higher f_{44} and lower f_{60} values with age. In our case there is a deflection from the nominal background value of 0.3%, portrayed by the vertical doted line, which coincides with the dates of the identified wildfires. Furthermore, when plotting the organic fragments at m/z 43 vs m/z 44 we observe the presence of less aged organic aerosol with higher f_{43} values during the same periods for most of the cases. The area between dashed lines of 1:1 and 2:1 is an indication of the presence of fresh OA.

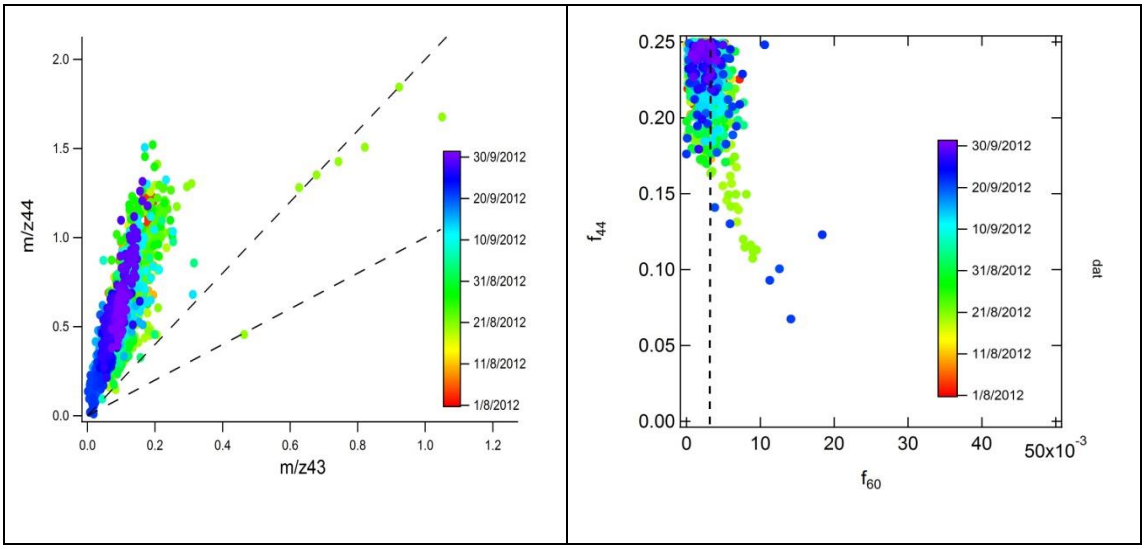

Figure SI-1.2: m/z44 vs m/z43 and f_{44} vs f_{60} for the whole measurement period, indicating the presence of biomass burning-influenced air masses.

Based on the approach of Sandradewi et al.[2] and by using an absorption exponent of 1.1 for pure traffic and the average value obtained in this study of 1.86 for pure wood burning conditions, we calculated the contribution of these components to total BC concentrations. The time series of each component is presented in Figure SI-1.3, where it can be seen that the identified biomass burning events are also depicted by the enhanced contribution of wood burning BC concentrations.

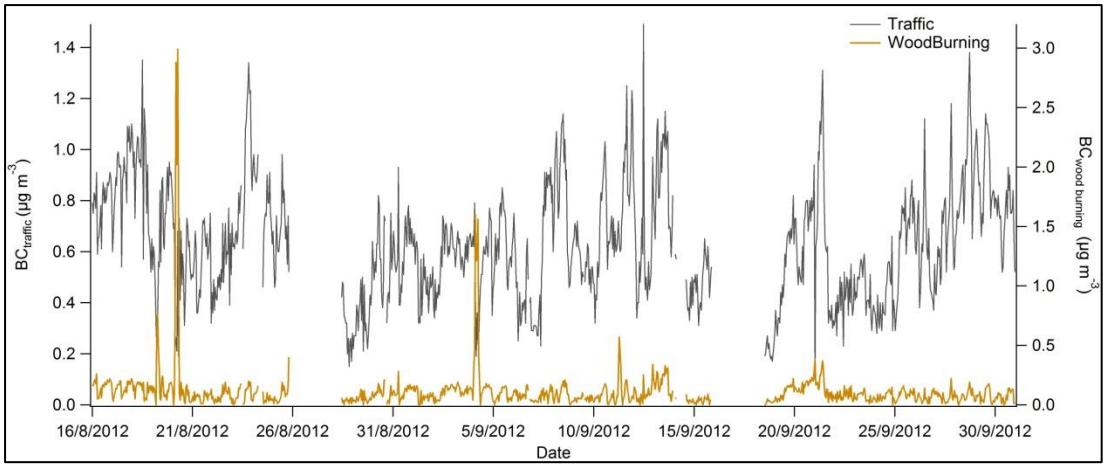

Figure SI-1.3: Estimated source apportionment of BC concentrations based on light absorption measurements.

SI-2 Comparison of ACSM versus filters

In Figure SI-2.1 the comparison between the concentrations measured by the ACSM are compared to those calculated from the filter analysis by Ion Chromatrography and the OC/EC Carbon Analyzer. The concentrations of sulphate and ammonium from ACSM are daily averaged to match the daily PM_1 filters time series. The ACSM concentrations are somewhat underestimated. For the conversion of OC to particulate organic matter (POM) a factor of 2.4 is used, which is derived from the ACSM measurements and the estimate of Aiken et al.[3]

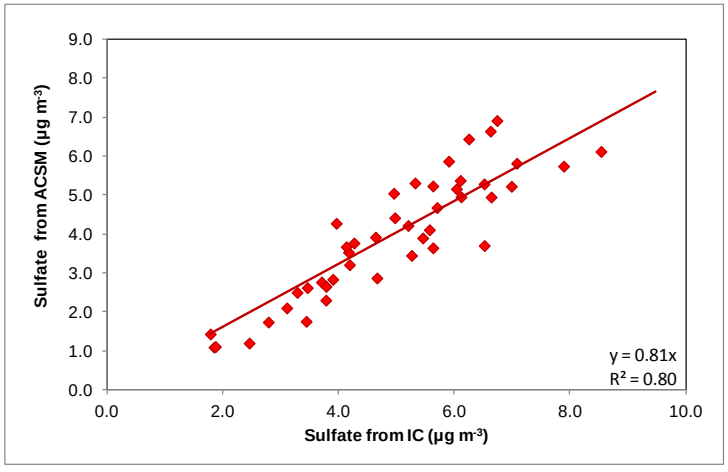

(a)

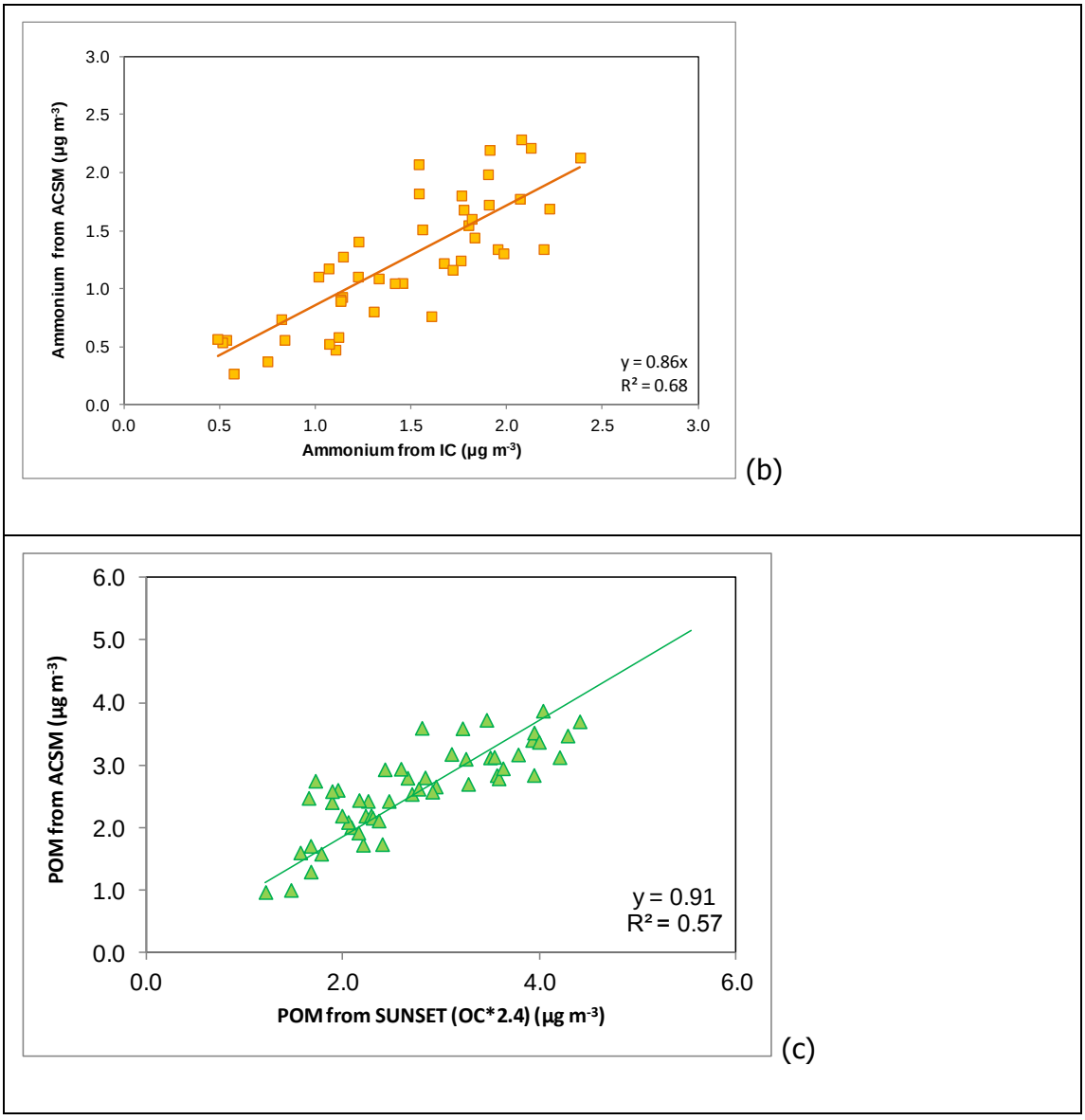

Figure SI-2.1: Inorganic species and organic matter comparison between ACSM, Ion Chromatography (IC) and OC/EC Carbon Analyzer (SUNSET Inc.): (a) sulfate, (b) ammonium, and (c) Particulate Organic Matter (POM).

Differences in concentrations can be attributed to errors and fluctuations in the collection efficiency of the species. For this reason we also studied the inorganic acidity of the sampled aerosol, which can be found in Figure SI-2.2, compared to nitrate concentrations. The acidic behaviour of aerosol in the area during summertime had also been observed by Hildebrandt et al.[4]

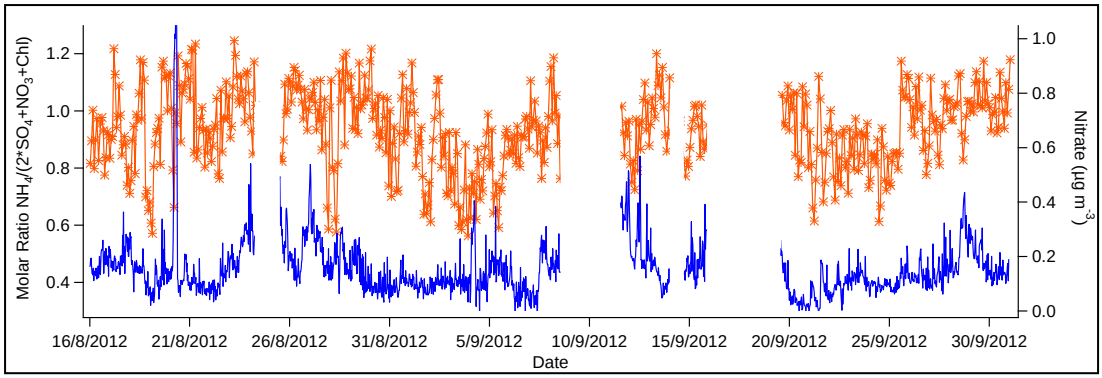

Figure SI-2.2: Inorganic acidity time series compared to nitrate concentrations.

SI-3 PMF Analysis

The organic aerosol components from the 2-month data set were extracted by performing Positive Matrix Factorization (PMF) analysis. PMF is a multivariate factor analysis technique developed by Paatero and Tapper[5] to solve the mass conservation problem of pollutant species with a bilinear model:

$$X_{ij\,measured} = X_{ij\,\mathrm{model}} + E_{ij\,\mathrm{model}} \; and \; X_{ij\,\mathrm{model}} = \sum_{p} G_{ip} F_{pj}$$

where the measured matrix X is approximated by the product of G and F and E is the residuals not fit by the model. Each column j of the matrix G represents the time series of a factor p, whereas each row i of F represents the profile (mass spectrum) of factor p. For aerosol mass spectrometry (AMS) data, $X_{ij\ measured}$ are the concentration of m/z j in time-step i, reconstructed by p factors having constant source profiles (F_{pj}) with varying contributions over the time period of the time period of the data set (G_{ip}). The entries in G and F are fit by the model using a least squares algorithm that minimizes iteratively the quantity Q^m, i.e. the residuals squared and weighted by the uncertainty[6,7].

The input organics and organics error matrices are derived automatically from the ACSM data analysis software, using a simple automated six-step process. First,

Organic mass spectrum matrix and its error are generated using the gain and dwell-time of the recorded data and error matrix is visually examined for reasonable average error values. Then variables with a weak signal are downweighted automatically by increasing the errors of m/z ratios with a scaling factor depending on the signal-to-noise ratio of each variable. The downweighted and non-downweighted errors with signal-to-noise ratio are, then, examined as a function of m/z. Finally, peaks related to m/z 44 in the fragment table are also automatically downweighted in order to avoid repetition of the information in m/z 44 several times, and at the final step the matrices are exported and saved in Igor text format so they can easily be loaded into an Igor experiment with the PMF procedures[8].

SI-4 PMF Results

SI-4.1 Q/Q_{exp} criterion

The presented Q/Q_{exp} plots correspond to "seed" and "f_{peak}" runs. As expected, diminishing values of this ratio for around 3-4 factors. From 1 to 2 factors there is a 27.4% decrease in the ratio, but from 2 to 3 and from 3 to 4 factors the decrease is the same (12.7 and 12.9%, respectively). Finally from 4 to 5 factors the Q/Q_{exp} almost reaches a plateau, with a mere 8% decrese. The results for the fpeak run were very similar (decrease of Q/Q_{exp} of 27%, 12.7%, 10.9% and 9.6%, respectively).

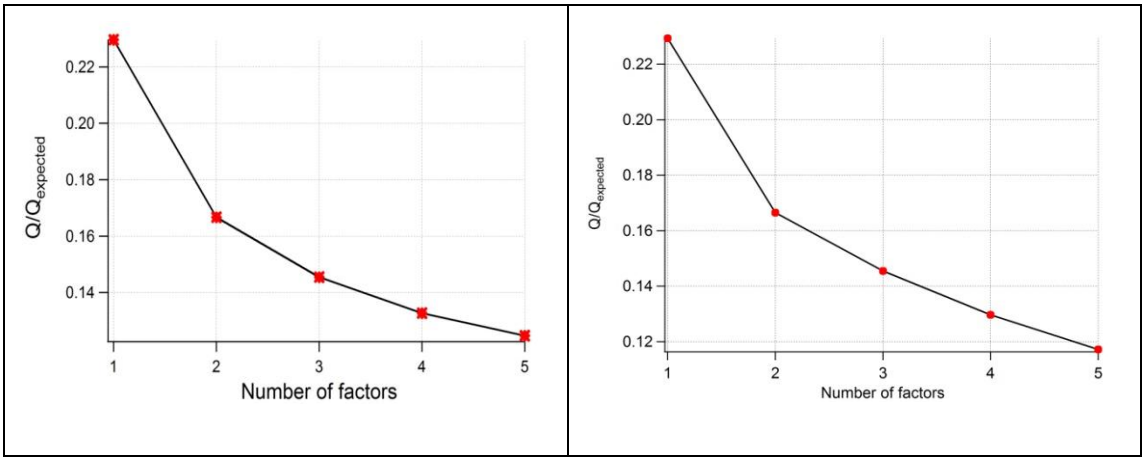

Figure SI-4.1: Q/Q_{exp} for different number of factors for seed run (left) and f_{peak} run (right).

SI-4.2 Seeds and f_{peak} variation

To investigate the stability of the solution and the possibility of local minima in the PMF solution space, the algorithm was initialized using 20 different starting points ("seeds"). Figure SI-4.2.1 shows the variation of the relative sources contributions and of the Q/Q_{exp} as a function of seed. The most stable solution is the 3-factor solution, with only one seed run out of twenty being substantially different. For the 20 different seed runs the Q/Q_{exp} values showed very little variability; correlation with external mass spectra was identical for the grand majority of the seeds (19 out of 20), and so was the contribution of each factor to the total organic mass, with no unexplained mass observed. Finally, the variation of each factor compared to the total variability was identical in almost all seed runs and unexplained variation was less than 20% with unexplained variation values being higher (greater than 30%) for m/z >100.

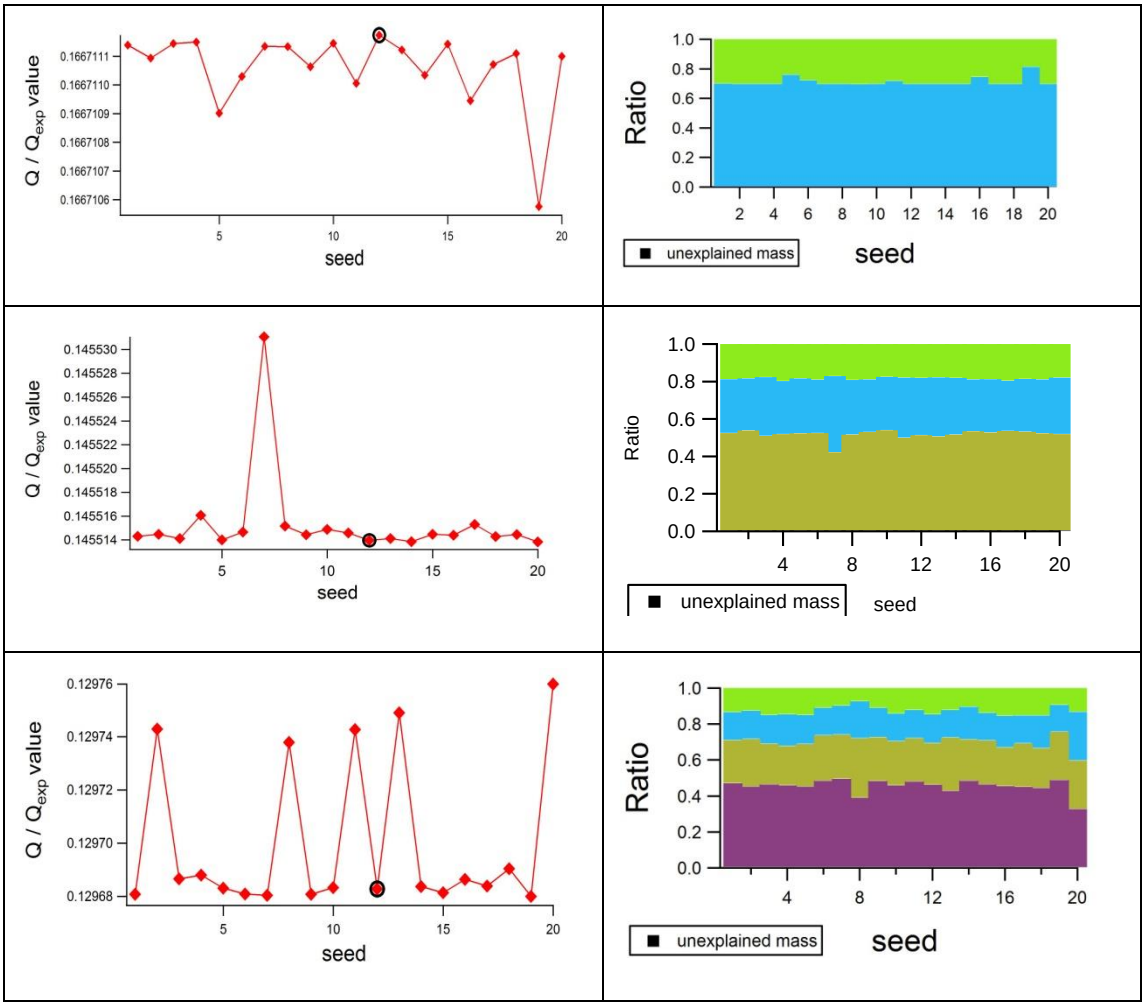

Figure SI-4.2.1: Relative factor contributions as function of different seeds for two-three-, and four-factor solutions.

In the case of the f_{peak} runs the respective graphs are illustrated in Figure SI-4.2.2. Once more there is no unexplained mass. The main observed difference is the ratio between negative and positive fpeak runs.

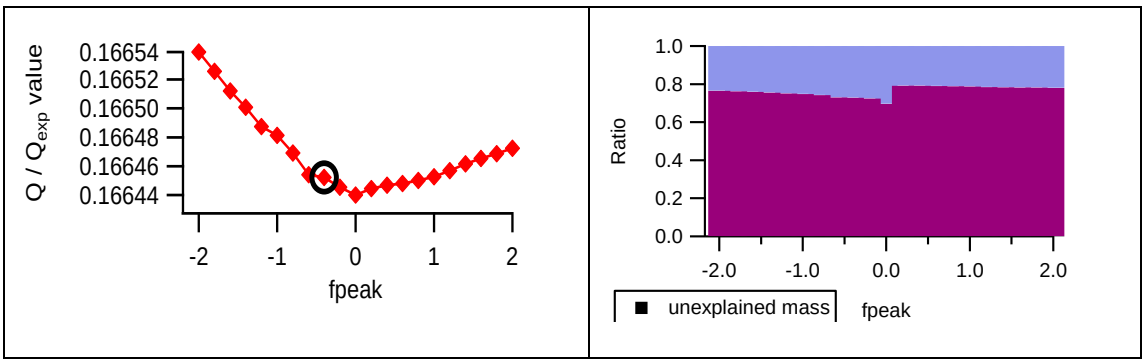

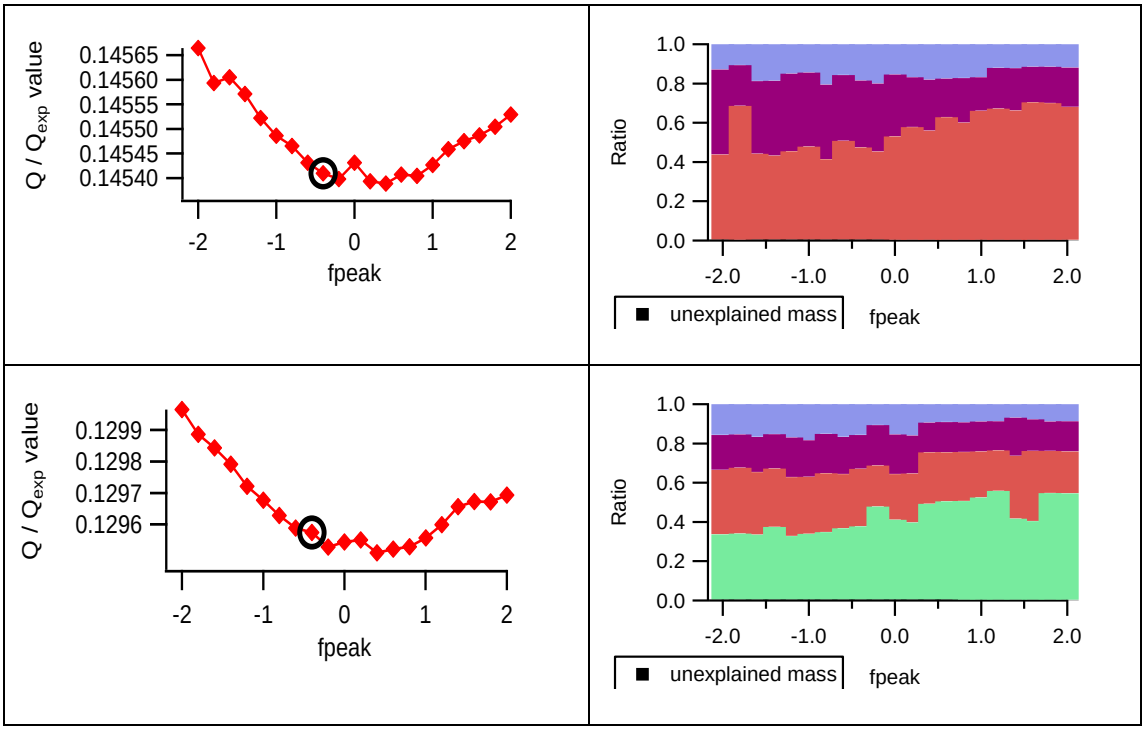

Figure SI-4.2.2: Relative factor contributions as function of different f_{peak} for two-three-, and four-factor solutions.

Based on the results of the f_{peak} runs, we compared the derived MS spectra for the 3-factor solution with external spectra (based on theta angles[9], Figure SI-4.2.3). The lowest difference in theta values for both BBOA as well as OOA between the derived f_{peak} spectra and the average BBOA and OOA found by Ng et al.[10] were found for f_{peak} -0.4 run. This f_{peak} run is used in all other comparisons.

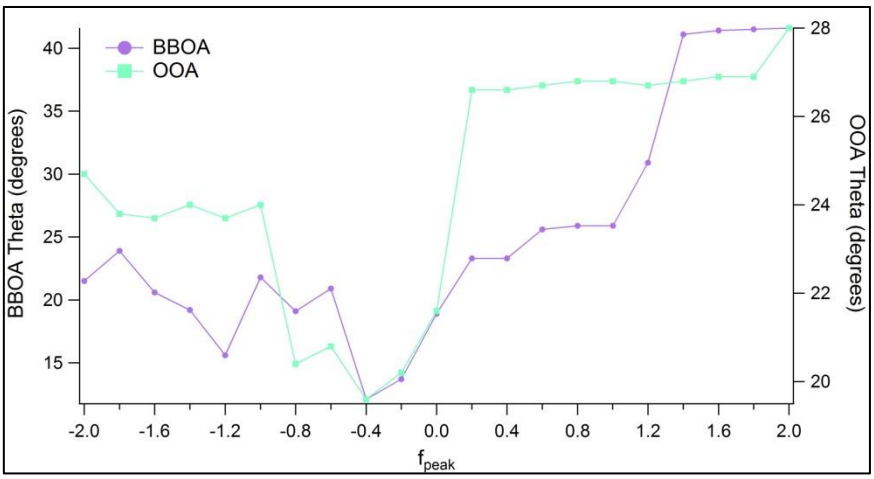

Figure SI-4.2.3: Criteria for the selection of the f_{peak}: we choose the f_{peak} for which the angle θ between the average BBOA and OOA found by Ng et al.[10] and the BBOA and OOA factor profiles from the f_{peak} run are minimum.

SI-4.3 Mass spectra and time series

In Figure SI-4.3.1 the mass spectra and time series for the two-factor, three-factor and four-factor solutions are presented. The selection of the solution was mainly based on the structure of the deconvolved mass spectra and correlation between the factor time series and various external tracers. For the case of 2 factors, one of the factors rather combines a BBOA profile with a more oxidized factor with a high contribution of m/z 28 and 44. This is the reason why the mass spectrum correlates both with BBOAavg[10] (theta angle 33.8) but better with average OOA[10] (theta angle 13.7). This combination is divided in two separate factors in the 3-factor solution: a more clear BBOA profile with a higher contribution of m/z 43 and an OOA profile which follows the BBOA time series and is probably a processed BBOA factor. Correlations with external spectra are also good (theta angle values around 15). Finally in the 4-factor solution the BBOA factor is split into 2 parts, factor 2 does contain m/z 18 or m/z 44 and their time series are also very similar. Correlation with external spectra is also poor: factor 2 has a theta angle of 26.5 compared to BBOA average spectra, factor 1 also correlates poorly with OOAavg[10], SVOA[11] and LVOA[12] (theta angles 23.9, 21.6 and 38.6, respectively).

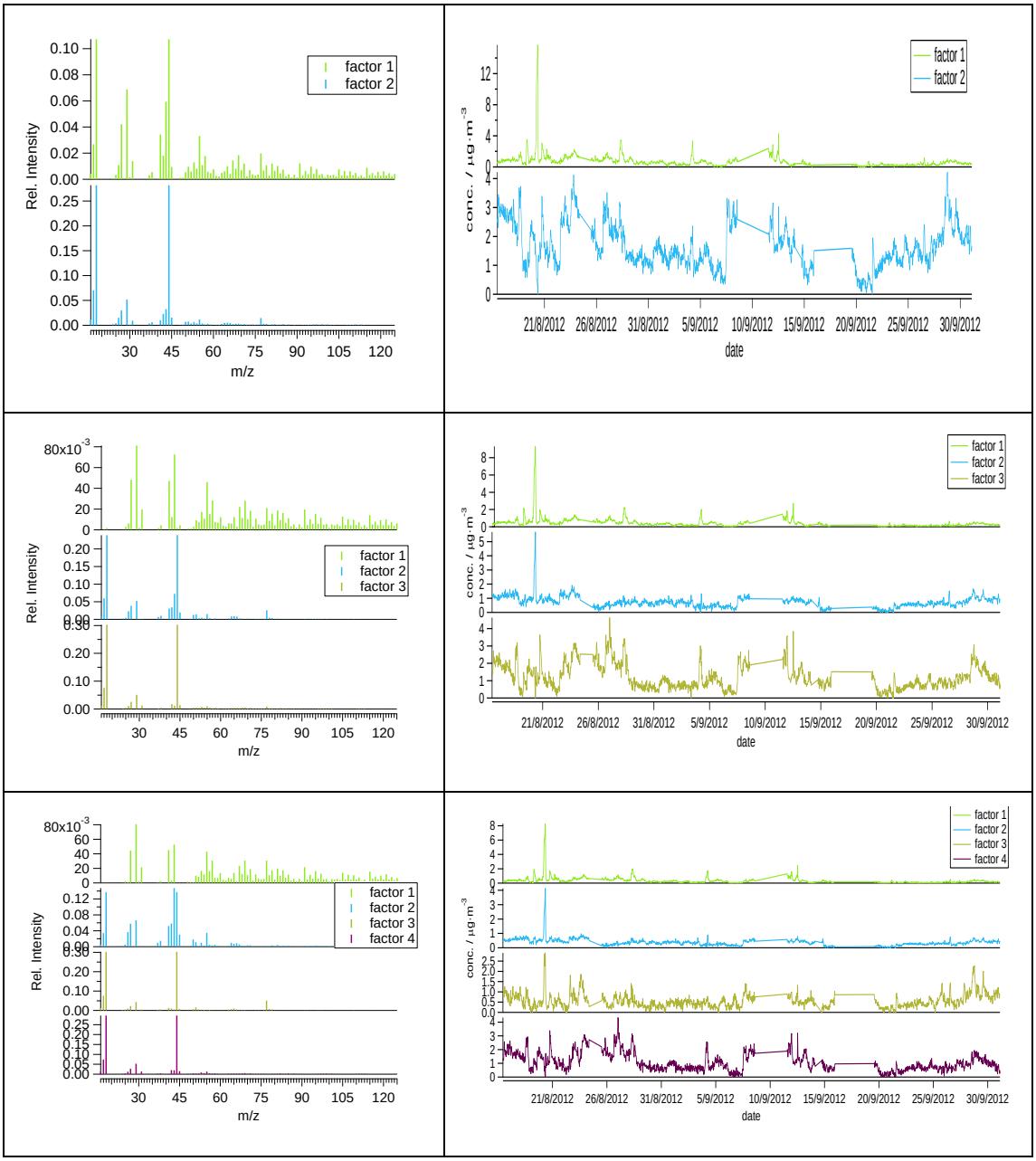

Figure SI-4.3.1: Mass spectra and time series for 2-factor, 3-factor and 4-factor PMF solutions for the seed run.

The respective mass spectra extracted from the f_{peak} run are presented in Figure SI-4.3.2. When comparing the different mass spectra derived by the 3-factor solution of the seed run and the f_{peak} run, the values are of 3.6 degrees for the BBOA, 4.5 for the OOA-BB and 0.3 for the OOA.

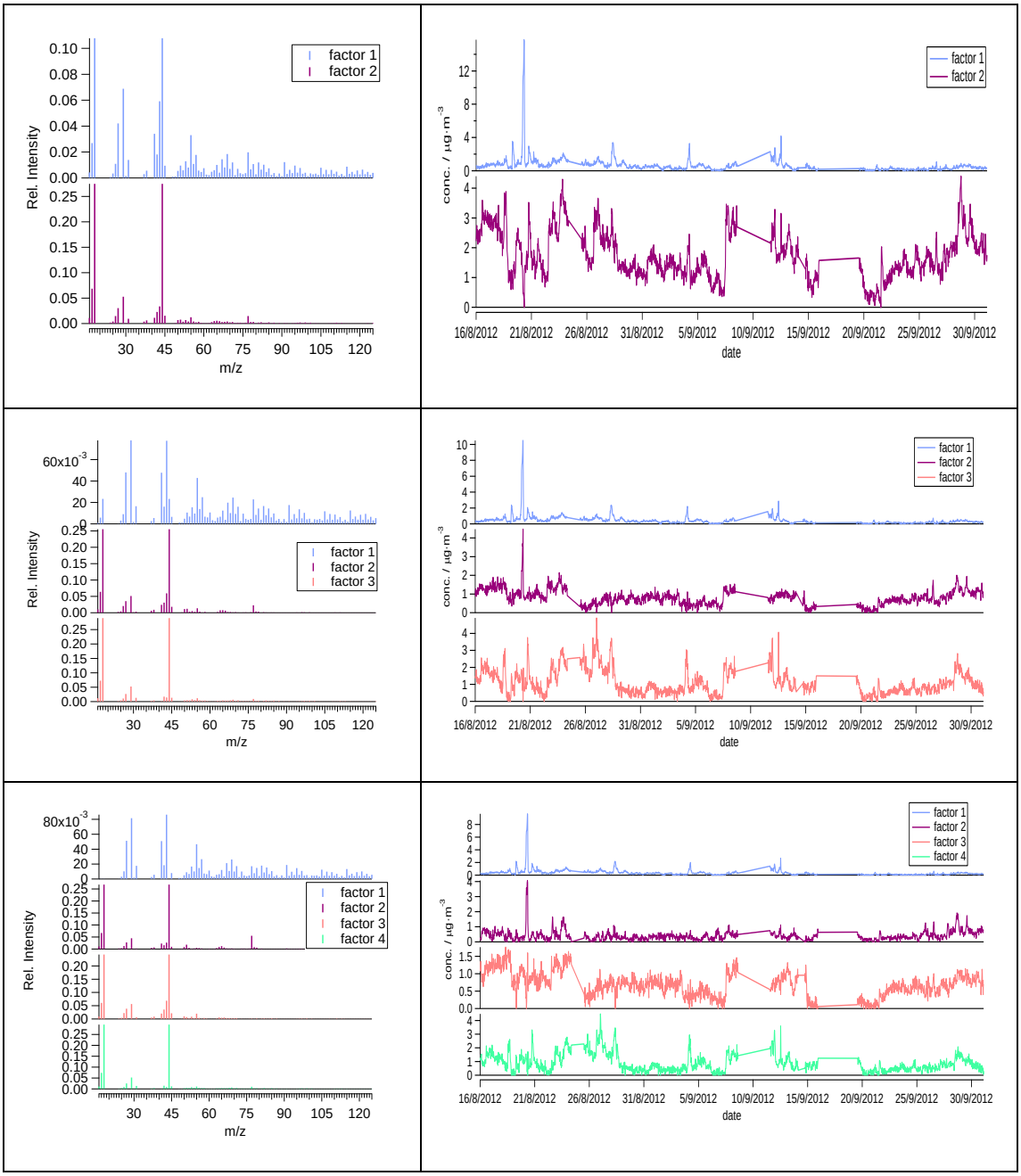

Figure SI-4.3.2: Mass spectra and time series for 2-factor, 3-factor and 4-factor PMF solutions for the f_{peak} run.

SI-4.4 Comparison of derived factors with external tracers

The timeseries of the derived factors were further compared to external tracers, such as BC, nitrate, sulfate and ammonium. The comparison for the two-, three- and four-factor PMF solution is presented in Table SI-4.4.1. The mixed BBOA-OOA (Factor 1) in the 2-factor solution correlates well with black carbon while OOA (Factor 2)

correlates better with sulfate. BBOA (Factor 1) in the 3-factor solution correlates well with BC and nitrate, OOA-BB (Factor 2) relatively well with BC and well with nitrate, while OOA (Factor 3) correlates better with sulfate and ammonium. Finally the splitting behavior of the 4-factor solution is once more evident as factors 1 and 2 exhibit the same behavior and so do factors 3 and 4.

2 factors	**BC**	**Nitrate**	**Sulfate**	**Ammonium**
Factor 1	0.6	0.74	0.02	0.08
Factor 2	0.33	0.46	0.66	0.71
3 factors	**BC**	**Nitrate**	**Sulfate**	**Ammonium**
Factor 1	0.62	0.75	0.02	0.08
Factor 2	0.41	0.63	0.29	0.38
Factor 3	0.43	0.47	0.59	0.62
4 factors	**BC**	**Nitrate**	**Sulfate**	**Ammonium**
Factor 1	0.62	0.75	0.02	0.08
Factor 2	0.47	0.63	0.14	0.21
Factor 3	0.52	0.66	0.49	0.54
Factor 4	0.39	0.53	0.48	0.53

Table SI-4.3.1: Comparison of the solutions derived from different number of factors with external tracers.

Once more, the f_{peak} run gives similar results with the seed run: in the 2-factor solution Factor 1 correlates well with BC and nitrate (R^2=0.61 and 0.75, respectively)

while Factor 2 correlates well with sulfate and ammonium (R^2=0.66 and 0.71, identical with the seed run). In the 3-factor solution factor 1 correlates well with BC and nitrate (R^2=0.6 and 0.73), factor 2 well with nitrate (0.58) and factor 3 with sulfate and ammonium (R^2=0.52 and 0.56, respectively).

SI-4.4 Comparison of derived spectra for each fire event

We performed separate PMF analysis for each fire event, selecting the corresponding 3-factor solution for each event and identifying the same profiles as for the whole measurement period (BBOA, OOA-BB and OOA). The time series of the three factors during the separate fire events along with the different BBOA spectrum of each event can be seen in Figure SI-4.4.1, color-coded by event. We present only the different BBOA spectra as the OOA-BB and OOA spectra did not exhibit remarkable differences (comparison can be found in table SI-4.4.3).

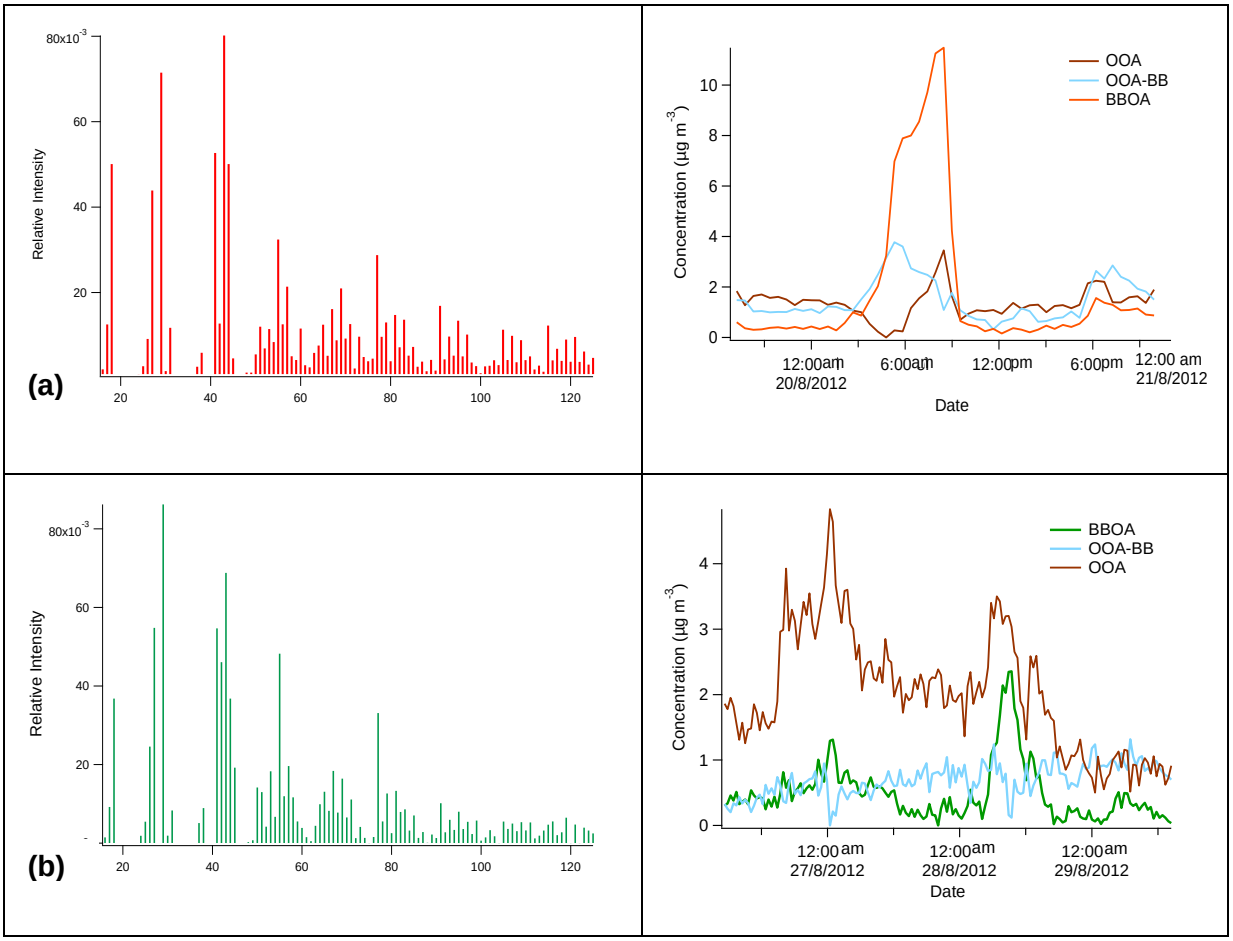

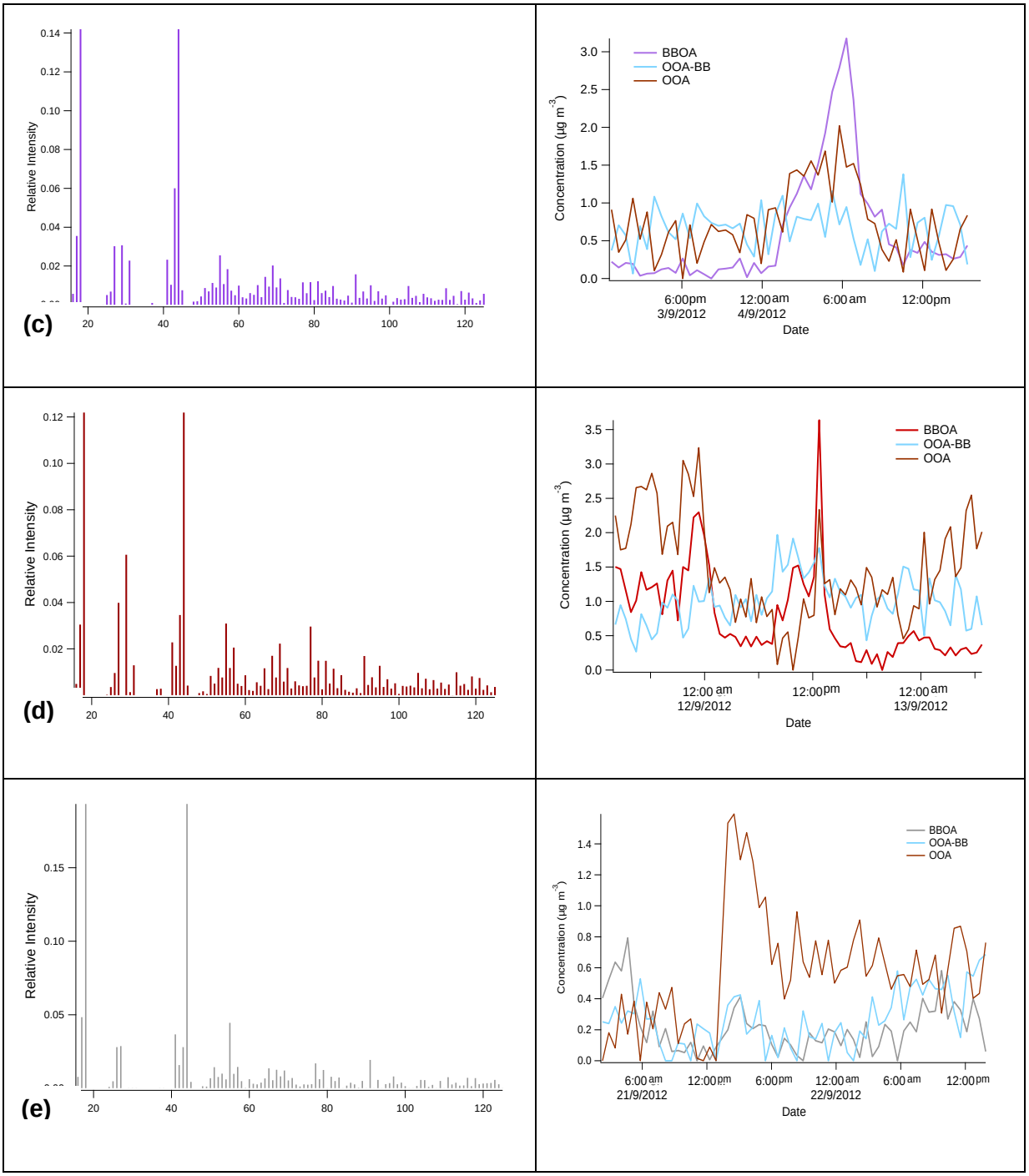

Figure SI-4.4.1: The different biomass-burning spectra and diurnal variability of factors derived for each fire event: (a) Chios, (b) Croatia, (c) Euboea, (d) Andros, and (e) Sicily.

The mass spectra from the separate PMF run for each fire event were also compared to external mass spectra, namely average BBOA spectra. We used the theta angle[8] to compare the mass spectra between the BBOA, processed-BBOA (OOA-BB) and

OOA of our study with different BBOA, OOA, SVOA and LVOA spectra found in AMS Spectral Databases. The results of the comparison are shown in the figure below, color-coded by the same colors used in the reported mass spectra for consistency.

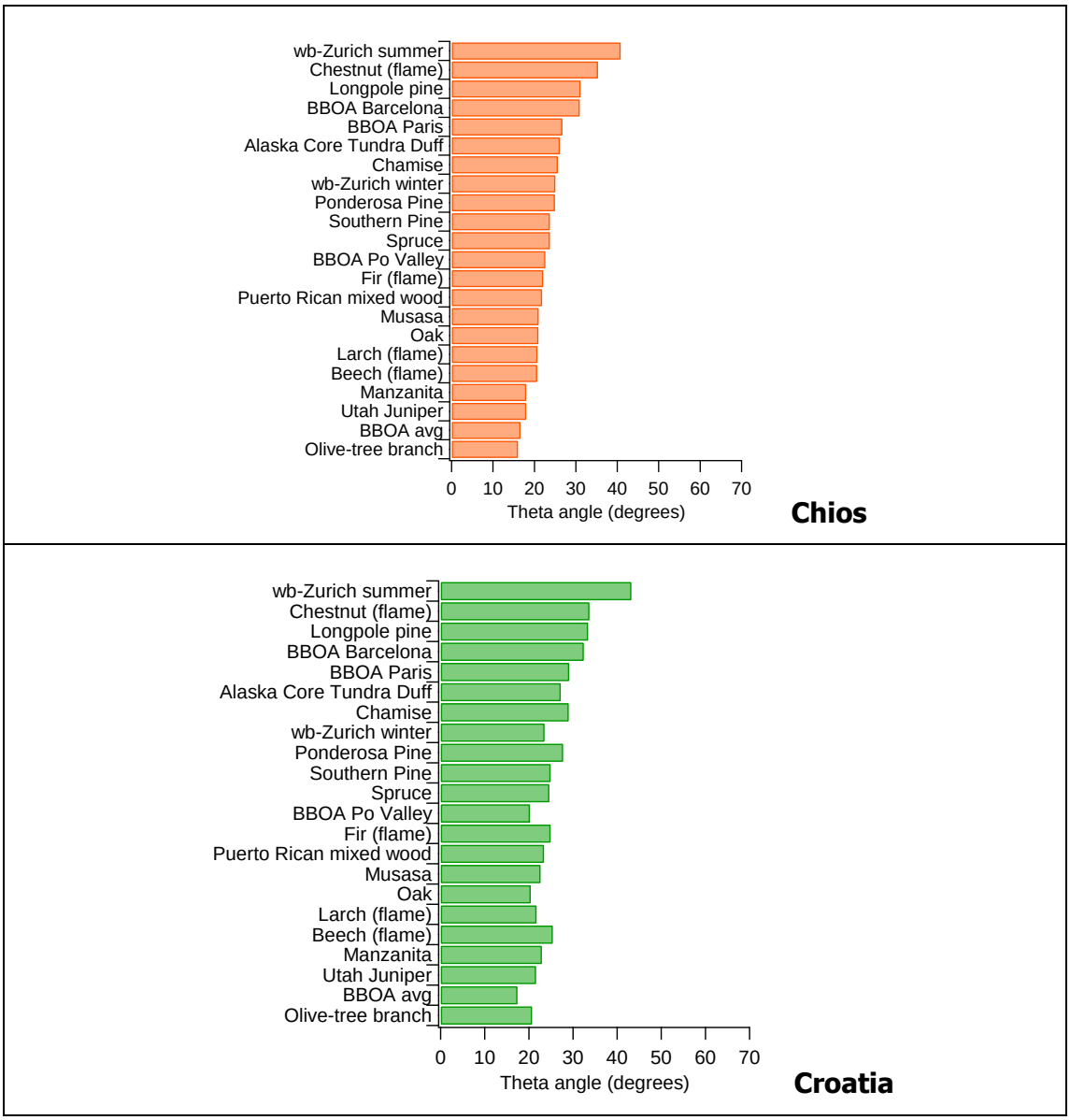

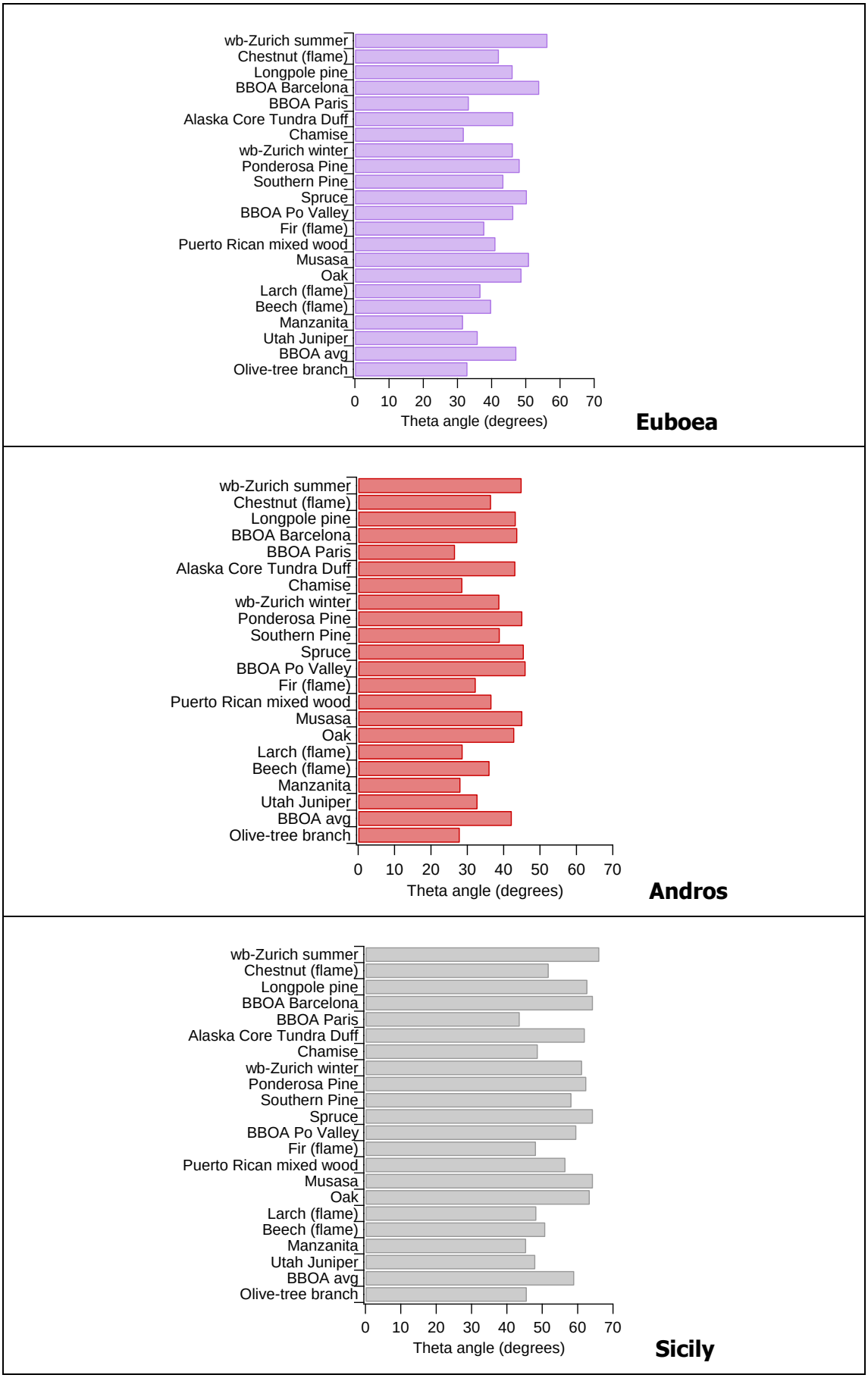
wb-Zurich summer
Chestnut (flame)
Longpole pine
BBOA Barcelona
BBOA Paris
Alaska Core Tundra Duff
Chamise
wb-Zurich winter
Ponderosa Pine
Southern Pine
Spruce
BBOA Po Valley
Fir (flame)
Puerto Rican mixed wood
Musasa
Oak
Larch (flame)
Beech (flame)
Manzanita
Utah Juniper
BBOA avg
Olive-tree branch
0 10 20 30 40 50 60 70
Theta angle (degrees)
Euboea
wb-Zurich summer
Chestnut (flame)
Longpole pine
BBOA Barcelona
BBOA Paris
Alaska Core Tundra Duff
Chamise
wb-Zurich winter
Ponderosa Pine
Southern Pine
Spruce
BBOA Po Valley
Fir (flame)
Puerto Rican mixed wood
Musasa
Oak
Larch (flame)
Beech (flame)
Manzanita
Utah Juniper
BBOA avg
Olive-tree branch
0 10 20 30 40 50 60 70
Theta angle (degrees)
Andros
wb-Zurich summer
Chestnut (flame)
Longpole pine
BBOA Barcelona
BBOA Paris
Alaska Core Tundra Duff
Chamise
wb-Zurich winter
Ponderosa Pine
Southern Pine
Spruce
BBOA Po Valley
Fir (flame)
Puerto Rican mixed wood
Musasa
Oak
Larch (flame)
Beech (flame)
Manzanita
Utah Juniper
BBOA avg
Olive-tree branch
0 10 20 30 40 50 60 70
Theta angle (degrees)
Sicily

Figure SI-4.4.2: Comparison of the different BBOA mass spectra for each fire event with different BBOA mass spectra

(Mass spectra source: http://cires.colorado.edu/jimenez-group/AMSsd/)

Te best correlation with the reference BBOA spectra is found for the fire events of Chios and Croatia, which exhibit also the highest relative intensity of f_{43}. Euboea and Andros show comparable theta angles relatively to the reference spectra. Finally, the poorest correlation is observed for Sicily, which is expected as both characteristic markers f_{60} and f_{73} have the smallest relative intensity of all fire events while f_{44} has the highest. Therefore aging of the BBOA will lead to OA that resembles more to OOA rather than to BBOA.

We also compared the different spectra of each 3-factor solution with the corresponding spectra of the rest of the fire events. The comparison of the processed-BBOA (OOA-BB) and the OOA can be found in the following Table SI-4.4.3, where individual spectra are also compared to the cumulative ones derived for the whole measurement period. We also compared the processed-BBOA with the OOA of each fire event to make sure they differ sufficiently. The theta values ranged from 14.9 degrees for the Croatia fire, to 16.5 degrees for Chios, 19.5 degrees for Andros, 22.9 degrees for Euboea and 18.7 degrees for Sicily. The values for the Croatia and the Sicily fires are expected to resemble, due to the longer transport time.

OOA-BB	Chios	Croatia	Euboea	Andros	Sicily
Chios		5.8	11.8	10.5	14.5
Croatia			13.5	13	16.3
Euboea				12.4	12.5

Andros					10.5
OOA-BB of whole period	15.5	18.7	19.1	7.5	16
OOA	Chios	Croatia	Euboea	Andros	Sicily
Chios		5.8	11.8	10.5	14.5
Croatia			13.5	13	16.3
Euboea				12.4	12.5
Andros					10.5
OOA of whole period	5.4	6.8	10.8	8.9	8.9
Transport time	7h	16h	9h	8h	33h

Table SI-4.4.3: Comparison of the different OOA mass spectra for each fire event with the rest of the fire events, as well as with the cumulative spectra for the whole measurement period.

SI-4.6 PMF solution residuals

The comparison between the model residuals for the two- to four-factors is presented in Figure SI-4.6. The results are given in a graph where the matrix of the residuals is scaled by the uncertainty (as a function of variable and time). White spaces denote data points where $|e_{ij}| < \sigma_{ij}$, while the red and blue points denote residuals that exceed the limit in positive and negative directions, respectively. Ideally the distribution of colors should be random and pattern-free, indicating that unexplained data is distributed randomly throughout the dataset.

It can be seen that when moving from the two- (a) to the three-factor solution (b), residuals are scaled better with uncertainty and less red and blue points are observed both in terms of the time series, as well as in terms of variables. The residuals in the four-factor solution are also better scaled with uncertainty, especially in the higher variables. Nevertheless, as two of the four factors were from the splitting of the BBOA factor of the 3-factor solution, we decided to choose the three-factor solution.

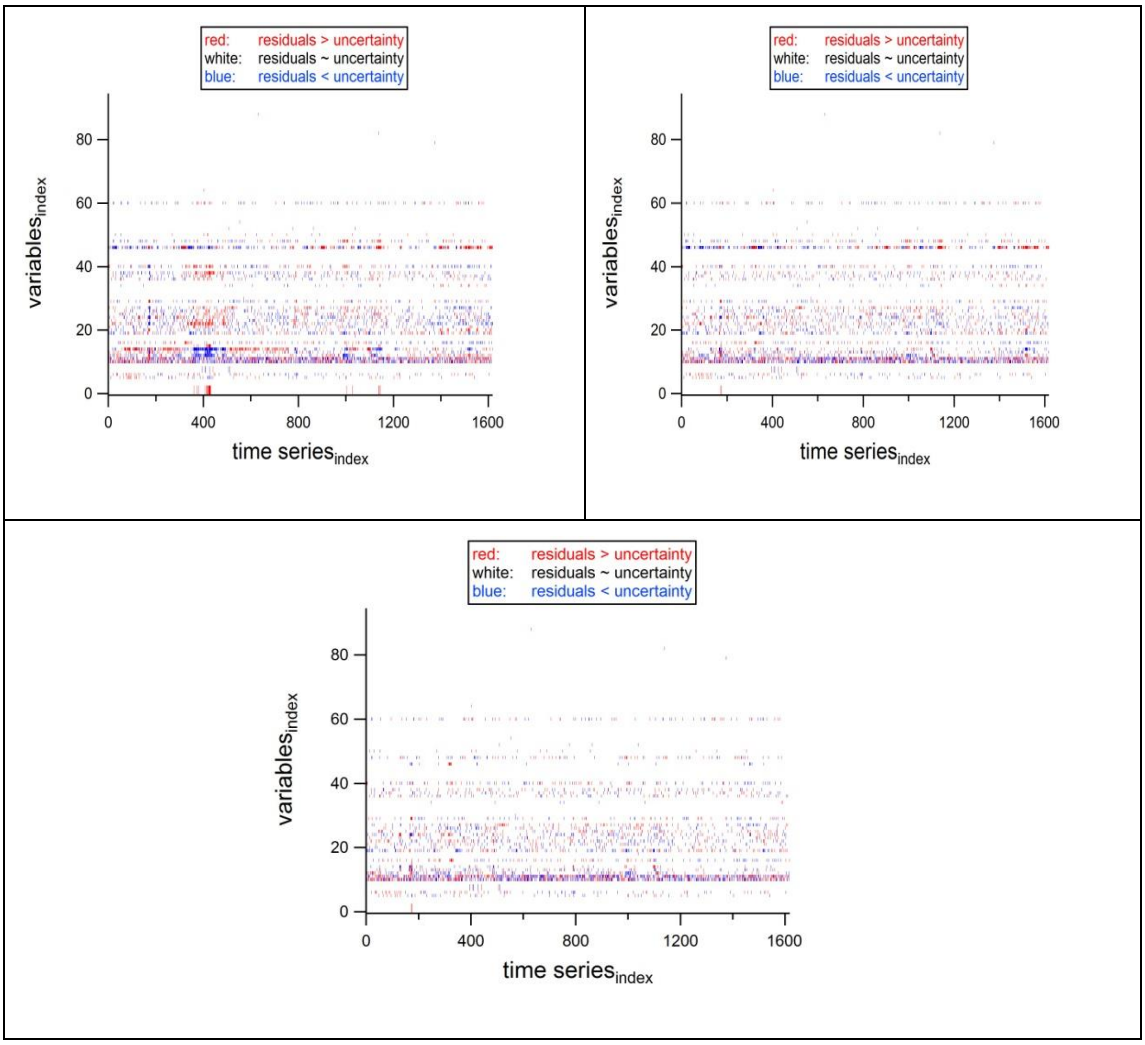

Figure SI-4.6: Comparison between residuals for the two-, three- and four-factor solution.

References

(1) Cubison, M.J.; et al. Effects of aging on organic aerosol from open biomass burning smoke in aircraft and laboratory studies, *Atmos. Chem. Phys.*, **2011**, *11*, 12049-12064.

(2) Sandradewi, J.; Prevot, A.S.H.; Szidat, S.; Perron, N.; Lanz, V.A.; Weingartner, E; Baltensperger, U. Using aerosol light absorption measurements for the quantitative determination of wood burning and traffic emission contributions to particulate matter, *Environ. Sci. Technol.*, **2008**, *42*, 3316-3323.

(3) Aiken, A.C.; et al. O/C and OM/OC ratios of primary, secondary, and ambient organic aerosols with high-resolution time-of-flight Aerosol Mass Spectrometry, *Environ. Sci. Technol.*, **2008,** *42*, 4478-4485.

(4) Hildebrandt, L., Engelhart, G.J., Mohr, C., Kostenidou, E., Lanz, V.A., Bougiatioti, A., DeCarlo, P.F., Prevot, A.S.H., Baltensperger, U., Mihalopoulos, N., Donahue, N.M., and Pandis, S.N.: Aged organic aerosol in the Eastern Mediterranean: the Finokalia Aerosol Measurement Experiment-2008, *Atmos. Chem. Phys.*, **2010**, *10,* 4167-4186.

(5) Paatero, P.; Tapper, U. Positive Matrix Factorization – a Nonnegative Factor Model with Optimal Utilization of Error-Estimates of Data Values, *Environmetrics*, **1994**, *5*, 111-126.

(6) Ulbrich, I.M.; Canagaratna, M.R.; Zhang, Q.; Worsnop, D.R.; Jimenez, J.L. Interpretation of organic components from Positive Matrix Factorization of aerosol mass spectrometric data, *Atmos. Chem. Phys.*, **2009**, *9*, 2891-2918.

(7) Ng, N.L.; Canagaratna, M.R.; Jimenez, J.L.; Zhang, Q.; Ulbrich, I.M.; Worsnop, D.R. Real-time methods for estimating organic component mass concentrations from aerosol mass spectrometer data, *Environ. Sci. Technol.,* **2011**, *45*, 910-916.

(8) Jayne, J.: Aerosol Chemical Speciation Monitor Data Analysis Software Manual, Aerodyne Research, **2011**.

(9) Kostenidou, E., Lee, B.-H., Engelhart, G.J., Pierce, J.R., and Pandis, S.N. : Mass spectra deconvolution of low, medium and high volatility biogenic Secondary Organic Aerosol, *Environ. Sci. Technol.*, **2009**, *43*, 4884-4889.

(10) Ng, N.L.; Canagaratna, M.R.; Jimenez, J.L.; Zhang, Q.; Ulbrich, I.M.; Worsnop, D.R. Real-time methods for estimating organic component mass concentrations from aerosol mass spectrometer data, *Environ. Sci. Technol.,* **2011**, *45*, 910-916.

(11) Hersey, S.P.; Craven, J.S.; Schilling, K.A.; Metcalf, A.R.; Sorooshian, A.; Chan, M.N.; Flagan, R.C.; Seinfeld, J.H. The Pasadena Aerosol Characterization Observatory (PACO): chemical and physical analysis of the Western Los Angeles basin aerosol, *Atmos. Chem. Phys.*, **2011**, *11*, 7417-7443.

(12) Crippa, M., DeCarlo, P.F., Slowik, J.G., Mohr, C., Heringa, M.F., Chirico, R., Poulain, L., Freutel, F., Sciare, J., Cozic, J., Di Marco, C.F., Elsasser, M., José, N., Marchand, N., Abidi, E., Wiedensohler, A., Drewnick, F., Schneider, J., Borrmann, S., Nemitz, E., Zimmermann, Jaffrezo, J.-L., Prévôt, A.S.H., and Baltensperger, U.: Wintertime aerosol chemical composition and source apportionment of the organic fraction in the metropolitan area of Paris, *Atmos. Chem. Phys.*, **13**, 961-981, 2013.